F-center formation in KI crystals under high-density optical excitation

Nobuko Ichimura[*]

*Department of Physics, Graduate School of Science, Osaka University, Machikaneyama-cho 1-1, Toyonaka City,
Osaka 560-0043, Japan*

Taketoshi Kawai and Satoshi Hashimoto

*Department of Physical Science, Graduate School of Science, Osaka Prefecture University, Gakuen-cho 1-1, Sakai City,
Osaka 590-0035, Japan*

The *F*-center formation in KI crystals under high-density optical excitation has been investigated at low temperature. The irradiation of the ArF excimer laser with the power level above $\sim$0.1 mJ/cm^2 creates the *F*-absorption band in KI crystals at 14 K, at which the *F*-center formation does not occur under the ordinary excitation. The *F*-center density under the high-density excitation has been analyzed by using the rate equations for the *F*-center formation. This analysis reveals that the generation rate of the *F* center depends on the second power of laser power. This fact verifies that the *F*-center formation occurs through a two-photon process, which suggests the interaction between two precursor centers leading to paired self-trapped excitons (STEs). On the other hand, the efficiency of the STE luminescence decreases and the additional decay components in the STE luminescence are newly observed under the same power level. As a result, it is deduced that both the reduction of luminescence efficiency and the appearance of the new decay components relate to the *F*-center formation through the two-photon process. The microscopic mechanisms for these phenomena have been discussed by using a simple rate-equation model which involves the paired precursor state and the paired STE state generated by the two-photon process. The present model has succeeded to explain qualitatively that the reduction of the luminescence efficiency and the appearance of the additional decay components relate closely to the *F*-center formation.

I. INTRODUCTION

Dense electronic excitation in insulators with strong electron-phonon coupling causes several atomic processes,[1] including defect formation,[2] crystal-to-amorphous transformation,[3] desorption of atoms from the crystal surface,[4] and heavy-ion track formation by energetic heavy ions.[5] In addition to the atomic processes above, self-trapping of carriers and/or free excitons (FEs) occurs in materials with strong electron-phonon coupling. The self-trapping of carriers and FEs induces the self-trapped excitons (STEs), accompanying localized distortion of atomic configuration in crystals. The phenomena such as self-trapping of excitons and defect formation are called photoinduced lattice relaxation.[6,7] Photoinduced atomic displacement in materials with strong electron-phonon coupling has been investigated as one of the most attractive studies in the physics of nonmetallic materials.

Alkali halide crystals, which are typical ionic crystals with strong electron-phonon coupling, have been extremely suitable for the experimental and theoretical studies of photoinduced atomic displacement, because various defect centers such as *F*, *H*, and V_k centers and the STE are easily created in the crystals by the irradiation with an electron beam, x ray, or ultraviolet (UV) light. Basic studies of radiation-induced point defects in alkali halides were performed by Castner and Kanzig.[8] They proved that the *H* and V_k centers are a hole center consisting of a halogen molecular ion X_2^- staying in the $\langle 110 \rangle$ direction in a single halogen site and staying at the center between two original anion sites

with its axis along a $\langle 110 \rangle$ direction, respectively. Kabler proved that the host-dependent broad luminescence bands due to the STE are the result of the recombination of a V_k center and an electron.[9]

The STE luminescence bands in alkali halides are polarized either parallel (σ) or perpendicular (π) to the majority σ axis of the aligned self-trapped holes. Thus, the STE luminescence has been classified into two categories at the beginning stage of the study, named as σ and π luminescence bands.[9,10] From the decay time, the σ and π luminescence bands originate from the allowed transition from a spin singlet STE state and the partially allowed transition from a spin triplet STE state, respectively.[11,12] Afterward, from the viewpoint of the lattice relaxation energy between the FE and the STE, the STE luminescence bands have been classified into three types (I, II, and III), which are proposed by Kan'no *et al.*[13] The classification is based on the relation of Stokes shift of the luminescence with the Rabin-Klick parameter S/D. S is defined as the space between adjacent halide ions along a $\langle 110 \rangle$ direction in the normal lattice and D is the diameter of the neutral halogen atom. From the study of the optically detected magnetic resonance,[14] three types of configuration of the STE were confirmed as follows. Type I STE is the on-center type and consists of a V_k center and an electron. Type III STE is the off-center type and is composed of the nearest-neighboring *F-H* pair. Type II STE is said to have the configuration between types I and III STE.

The correlated behavior of STE luminescence quenching and *F*-center formation in six alkali halides (LiCl, NaCl, Li Br, NaBr, KI, and RbI) was summarized early on by Pooly
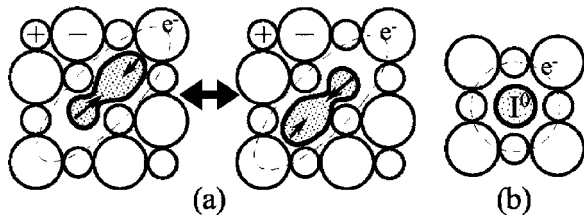
FIG. 1. (a) Wavering STE and (b) one-center self-trapped center.

and Runciman.[15] With increasing temperature in a particular temperature range, the F-center formation markedly increases and the π luminescence intensity decreases. Therefore, it was thought at the beginning stage that the F centers are evolved from the thermal activation of the lowest triplet state of STEs. However, the time-resolved studies of picosecond and femtosecond time regimes in alkali halides have revealed that the thermal conversion mechanism is not an entirely satisfactory model and precursor states exist before the relaxation to the triplet STEs and/or F centers.[16–19]

In alkali halides with $S/D \geq 0.45$, the yield of F-center formation (R_F) is nonzero at low temperature. It is said that F centers are directly and stably generated through the lattice instability induced by electronic excitation.[20,21] However, the femtosecond spectroscopic studies and *ab initio* calculations have revealed that the relaxation processes of e-h pairs have two distinct stages.[19,22–24] In the first stage within 6 ps after excitation, the transient hole centers are generated, and their interaction with electrons results in the fast formation of the F-H pair. Before the second stage of the relaxation, the F-H pair takes an intermediate state which is ascribed to a self-trapped hole center and an electron interacting each other with nearly on-center configuration. This state is said to be the wavering STE, as shown in Fig. 1(a). The second stage, which lasts over 100 ps at low temperature, comprises the off-center relaxation of the on-center STE formed in the first stage. This off-center relaxation brings the off-center STEs and the F centers.

In alkali halides with $S/D \leq 0.45$, R_F and the yield of the π luminescence are anticorrelated. At low temperatures, F centers are not formed transiently and stably, and the main relaxation of e-h pairs leads to the STEs.[16–19,21,25] The F-center formation occurs above ~ 100 K.[26,27] The study of picosecond spectroscopy has indicated the existence of a much faster growth process of F centers than the decay time of the triplet STEs above ~ 100 K.[16] This result implies that the other mechanisms play important roles in the temperature-dependent yield of the F-center formation. In the study of the femtosecond spectroscopy, a new broad absorption appears with a rapid rise of a few picoseconds, followed by a partial decay until about 10 ps. At low temperature, the broad absorption band subsequently develops the triplet STE band.[22] In the case of KI and RbI, the peak position of the broad absorption band coincides very well with that of the one-center self-trapped center deduced from the quantum-mechanical cluster calculation. The configuration of one-center self-trapped state is schematically illustrated in Fig. 1(b). The one-center self-trapped state can be regarded as a precursor state of the triplet STE. In the case of NaCl,

above ~ 100 K, with the decay of the broad absorption band, the absorption bands due to both the triplet STE and F center are observed. The configuration of the new center exhibiting the broad absorption band is described as a population of relaxing excitons around off-center configurations, which is similar to the configuration shown in Fig. 1(a). The new center can be regarded as a precursor state which is common to both the triplet STE and F center in NaCl.

The F-center formation never occurs at low temperature under the ordinary excitation in alkali halides with $S/D \leq 0.45$. However, the specific excitations such as cascade excitation, dense excitation, and heavy-ion bombardments induce the F-center formation at low temperature. Such excitation would induce exciton-exciton interaction which does not occur under ordinary excitation.

In the cascade-excitation spectroscopy, the first pulse irradiation under the band-gap excitation generates the lowest triplet state of STEs, and the second pulse irradiated within the lifetime of the triplet STE excites the lowest triplet STE to the highly excited state of STE.[5,28–32] According to the previous study, the cascade excitation of the triplet STE in KI made the FE and σ luminescence bands increase.[29,30] However, the cascade excitation in alkali iodides does not lead to defect formation at low temperature.

In RbI, dense electronic excitation induces the interaction between FE and STE leading to the F-center formation and an extra luminescence in addition to the ordinary luminescence at low temperature.[33,34] The peak position of the extra luminescence is quite different from that of the STE luminescence. The decay constant of the extra luminescence is 100 ns which is much faster than that of the π luminescence (13 μs). Since the intensities of the F-absorption band and the extra luminescence band are proportional to the square of excitation intensity, it has been concluded that the appearance of the extra luminescence band and the F-center formation arise from the interaction between FE and STE.

Under heavy-ion bombardments, the intrinsic luminescence yield in alkali halides decreases with the increase of the stopping power,[5] and the F centers are generated even at low temperature. Large stopping power means that the excitation density is large. The decrease of the luminescence yield is due to the interaction between STEs which enhances the nonradiative decay of STEs. In addition, two neighboring STEs are considered to be converted into an F center under extremely dense excitation in ion tracks. However, the experimental evidence which supports the interaction between STEs has not been reported. The electronic process under ion bombardment is very complex and the microscopic mechanism of exciton relaxation is not clear.

In this paper, we present the F-center formation and the STE luminescence properties in KI crystals at low temperature under high-density optical excitation. Alkali iodides are the most interesting crystals among all alkali halides because both FE and STE coexist and there are all types of STEs.[35–39] At low temperature, the F center cannot be generated under weak excitation in alkali iodides (NaI, KI, and RbI). Nevertheless, in RbI under the high-density optical excitation, the F-center formation at low temperature occurs with the appearance of an extra luminescence band.[33,34] This result implies that the high-density excitation leads to the new phe-

nomena due to the interaction between high-density excitons. From the comparison between RbI (0.40) and KI (0.33) in the Rabin-Klick parameter, the *F* center is not easily formed in KI than in RbI. It is worthy to confirm whether the *F*-center formation also occurs in KI at low temperature under the high-density excitation. Then, in order to make clear the interaction between the high-density excitons, further experiment on luminescence properties under the high-density optical excitation should be performed. In this study, the excitation intensity on the sample has been widely changed from a very weak level to an extremely intense one in which the crystal surface is seriously damaged. The change of optical properties over the very wide range of the excitation intensity has never been reported in alkali halides.

The present paper is organized as follows. The sample preparation and measurements of optical spectra are described in Sec. II. In Sec. III, the *F*-center detection in KI at 14 K under the high-density excitation is analyzed by using the rate equations. The power dependence of intrinsic luminescence bands has been measured, which is shown in Sec. IV. Finally, in Sec. V, we discuss the exciton interaction by using a simple rate-equation model which is the basis of the mechanism of dynamical instability of *e-h* pairs.

II. EXPERIMENTAL PROCEDURE

The samples used in the present study were thin crystals grown from melt in a small gap of a cell which was made of a couple of two transparent plates, as shown in Fig. 2(a).[40] We used sapphire single crystals as the cell material because the sapphire plates are quite transparent until the vacuum UV region and are hardly affected by intense laser irradiation.

The sample crystal of KI was grown as follows. A small fragment of bulk KI crystal was placed on the step and inserted into the small furnace, shown in Fig. 2(b). The bulk KI crystal was obtained from the crystal-growth laboratory of Utah University. Above the melting temperature of 681 °C, the melt was introduced into the gap through capillarity or surface tension in N_2 ambient gas. The thickness of the thin KI crystal involved in the cell was usually more than 10 μm. The samples grown have an advantage that sapphire plates prevent the desorption of atoms from the surface under laser irradiation of high powers. Purity of the starting bulk crystal is very high. Thin crystals obtained show no emission bands due to residual impurities even under the very-high-density excitations.

An ArF excimer laser (Lambda Physik COMPex 102) of 193 nm (6.42 eV) with the pulse duration of 15 ns and the pulse repetition of 10 Hz was used in the present study. The photon energy of the laser corresponds to that of the band-to-band transition region of KI. From the absorption coefficients of KI at this photon energy (2.1×10^5 cm^{-1}), the penetration depth of the laser light is only 0.05 μm in case of weak excitation, which is much smaller than the crystal thickness of more than 10 μm.[41] The penetration depth of the ArF excimer laser never exceeds more than 10 μm under the irradiation with the maximum laser power. Thus, almost all photons irradiated are absorbed near the surface of KI.

We investigated the laser power dependence from 10^{-3} to 50 mJ/cm^2 per pulse. The laser power was measured
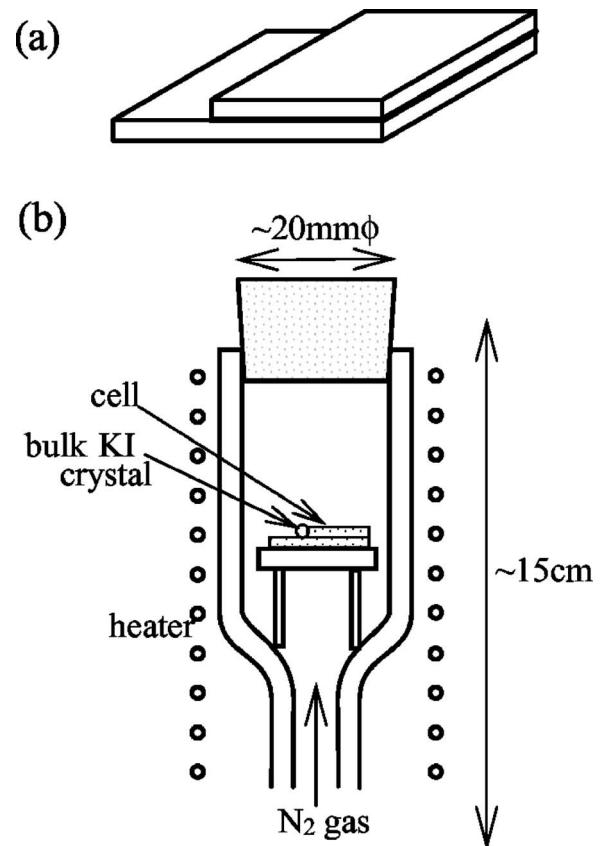
FIG. 2. (a) Schematic illustration of a cell made of two sapphire plates. The size of the lower plate is $8 \times 15 \times 1$ mm^3 and that of the upper plate is $8 \times 11 \times 1$ mm^3. (b) Schematic illustration of a small furnace for growing a thin crystal using the cell shown in (a).

by the pyroelectric Joule meter having the irradiated area of 1 cm^2. The maximum laser power was attenuated by several quartz plates which had the transmittance of about 50% or by reflecting the laser light using a few quartz plates, whose reflectance was about 10% at 193 nm. The cells were wrapped in an aluminum foil. The window was cut in the size of about 2×3 mm^2 through the aluminum foil. The beam size of the ArF excimer laser was about 1×3 cm^2, which was much larger than the window size. Thus, it was recognized that the sample was uniformly irradiated with the unfocused laser light.

The arrangement for the measurement of the absorption spectra before and after the irradiation by the ArF excimer laser is shown in Fig. 3. D_2 or *W* lamp was used for the measurements of the absorption spectra. The measurements were done by a detection system consisting of a grating monochromator (MS257TM) and an intensified charge-coupled device (CCD) detector (ORIEL Instruments). The measurements and laser irradiations were performed at 14 K.

In the present study, the absorption spectra of the *F* band were mainly investigated. Since the thickness of colored region due to the *F* centers was very thin, $\sim$0.05 μm, the absorbance was also very small. In order to evaluate such small absorbance, we had to detect the difference of the transmitting light intensity very carefully. The measurable minimum absorbance was about 0.0005 in optical density,
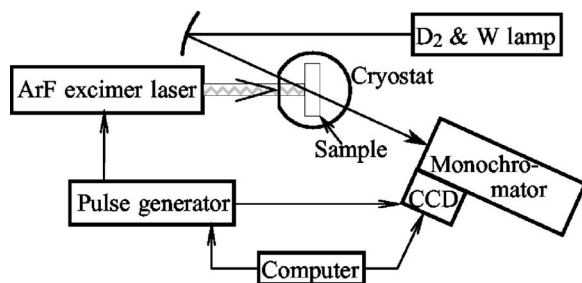
FIG. 3. Optical system for measuring the absorption in the KI crystal before and after irradiation of the ArF excimer laser.

and then the observed minimum density of the F centers was estimated by using Smakula's equation,[10]

$$N_F(\text{cm}^{-3}) = 0.87 \times 10^{17} \frac{n}{(n^2+2)^2} \frac{\mu W}{f}, \qquad (1)$$

where N_F is the density of the F centers, n is the refractive index of KI at the peak wavelength of the F band ($n = 1.66$ at 656 nm),[42] μ is the absorption coefficient at the peak of the F band in cm^{-1}, W is the half width of the F band in eV, and f is the oscillator strength of KI ($f = 0.83$).[43] μ is determined by the absorbance A and the effective thickness of the sample d from the following relation:

$$\mu(\text{cm}^{-1}) = \frac{1}{\log_{10} e} \frac{A}{d}. \qquad (2)$$

From the absorption spectrum, we obtain the minimum density of the F centers as about 3×10^{17} cm^{-3}, where $d = 0.05\ \mu$m.

As the thickness of the crystal was more than 10 μm, small interference fringes were seen in the visible region of the absorption spectrum. However, the effect of the interference fringes was so small that it eventually made no effect on the measurement.

The measurements of the luminescence spectra under excitation of the ArF excimer laser were done by a detection system consisting of a mirror, a lens, a monochromator, and an intensified CCD. In order to observe the time-resolved luminescence spectra, the timing for the oscillation of the ArF excimer laser and the gate position of the CCD detector were controlled by a pulse generator (DG535). The minimum gate width of the CCD was 7 ns. The luminescence spectra obtained were corrected for the wavelength dispersion of the monochromator and for the spectral response of the detection systems. The time-integrated luminescence spectra were detected by the CCD whose gate was opened during a sufficiently longer time than the decay time of luminescence bands. The decay profile of the luminescence intensity at a specific wavelength was obtained from the time-resolved luminescence spectra at any delay time after the laser excitation.

III. DETECTION OF F-CENTER FORMATION

A. Absorption spectra

In alkali iodide crystals, it is usually accepted that the F centers are not formed under conventional excitation levels
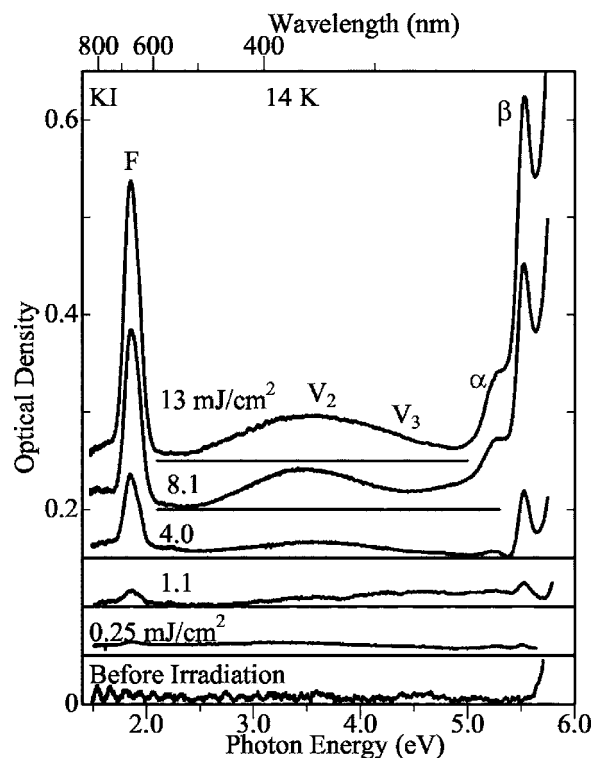
FIG. 4. The absorption spectra of the thin KI crystal before and after laser irradiation with various power levels at 14 K. Laser powers are indicated in the figure. The number of shots irradiated is 1000.

at low temperatures. We have succeeded to create the F centers in the KI crystal at low temperature under the high-density excitation of an ArF excimer laser.

Figure 4 shows the absorption spectra of KI before and after laser irradiation with various power levels at 14 K. Before laser irradiation, any absorption band is not seen below ~ 5.5 eV, which is shown in the bottom of Fig. 4. The rise of the absorption above ~ 5.7 eV corresponds to the intrinsic absorption edge of the KI crystal. The small interference fringes between 1.5 and 3.2 eV arise from the small gap of two sapphire plates. After laser irradiation of 1000 shots, several absorption peaks appear and the interference fringes in the visible region can hardly be seen, as seen in Fig. 4. The absorption peak showing the F-center formation is clearly observed at 1.86 eV and its peak intensity increases with increasing laser power.

The absorption bands peaking at 5.22 and 5.53 eV are usually assigned as α and β bands, respectively. The α and β bands are attributed to the exciton bands perturbed by the anion vacancy and the F center, respectively.[44] A broad band peaking around 3.5 eV consists of two absorption bands due to the V_2 (3.5 eV) and V_3 (4.5 eV) centers which are nearly $\langle 100 \rangle$-oriented I_3^- molecular ions.[45,46]

The excitation power employed in the present study is by far larger than that in the previous experiments performed in KI under the irradiation of pulsed electron beam[21,44] and picosecond[17] and femtosecond laser lights.[19] For example, in the case of the irradiation of pulsed electron beam, the energy density per electron pulse ranged from about
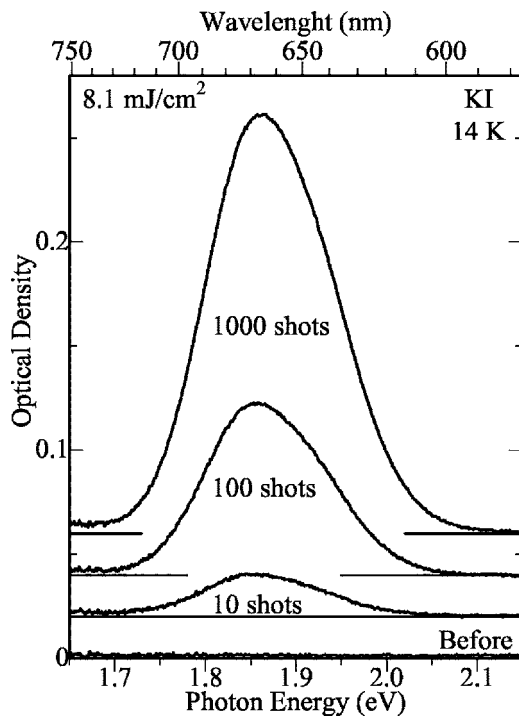
FIG. 5. Absorption changes of the *F* band with increasing number of shots. Laser power is 8.1 mJ/cm^2. The irradiated numbers are indicated in the figure.

10^{15} to 10^{16} eV/cm^2 at the crystal surface. The penetration depth of the pulsed electron beam was about 500 μm. On the other hand, the energy density of the ArF excimer laser per pulse ranges from $\sim 10^{13}$ to 10^{16} eV/cm^2 at the crystal surface. The penetration depth of the ArF excimer laser is estimated to be 0.05 μm, taking into account the absorption coefficient of KI at 193 nm. Because the photon energy of the ArF excimer laser corresponds to the intrinsic absorption region, the penetration depth of laser light is much smaller than that of the electron beam. Thus, the excitation density of the ArF excimer laser is 10^2–10^4 times as large as that of the pulsed electron beam.

In the study of picosecond and femtosecond spectroscopies, the two-photon absorption process was employed to generate *e-h* pairs. The absorption coefficient of two-photon absorption at unresonant wavelength is known to be of the order of 1 cm^{-1}, while the absorption coefficient at 193 nm of the ArF excimer laser is $\sim 10^5$ cm^{-1}.[41] Thus, the excitation density of the ArF excimer laser is by far higher than that of short-pulse lasers.

B. Power and shot-number dependence of *F*-center formation

The density of the *F* centers created under laser irradiation depends on the power and the number of shots. We have investigated the dependence of these two factors separately. Figure 5 shows the *F* absorption bands for various numbers of shots under the irradiation of 8.1 mJ/cm^2. The absorption intensities of the *F* bands become large with increasing number of shots. The density of the *F* centers have been estimated by using the Eqs. (1) and (2). In this condition, the
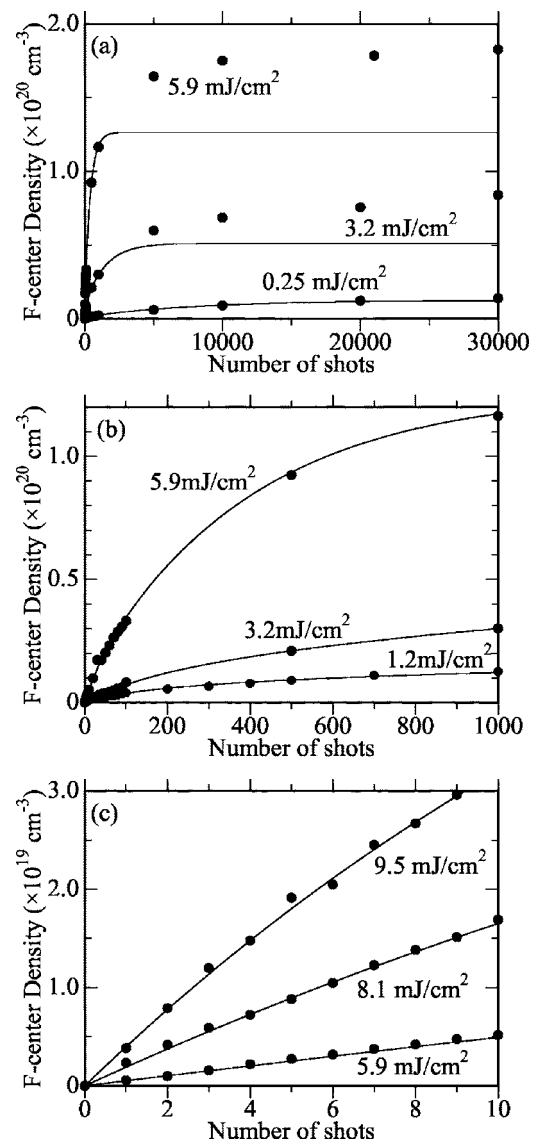
FIG. 6. The *F*-center density as a function of the number of shots at various laser powers. The maximum number of shots in (a), (b), and (c) is 30 000, 1000, and 10 shots, respectively. Closed circles are the experimental results. Solid lines are fitting results obtained from Eq. (6). Powers are denoted in the figures.

F-center density is 1.7×10^{20} cm^{-3} at 1000-shot irradiation.

In Figs. 6(a)–6(c), the density of the *F* centers is plotted against the number of shots between 0 and 30 000 shots, 0 and 1000, and 0 and 10 shots, respectively, under the irradiation with various levels of laser powers. The *F*-center density increases with increasing number of shots and becomes almost saturated in the region of a large number of shots, as seen in Fig. 6(a). The saturated density is dependent on the laser power and increases with increasing laser power.

The *F*-center densities after 30 000-shot irradiation (open circles) and for the first shot (closed circles) are plotted as a function of laser power in Fig. 7. Below ~ 2 mJ/cm^2, the *F*-center density for the first shot is determined by extrapolating the data, assuming the linearity of the *F*-center density against the number of shots. Between 0.1 and ~ 20 mJ/cm^2, the *F*-center density after 30 000-shot irradiation increases
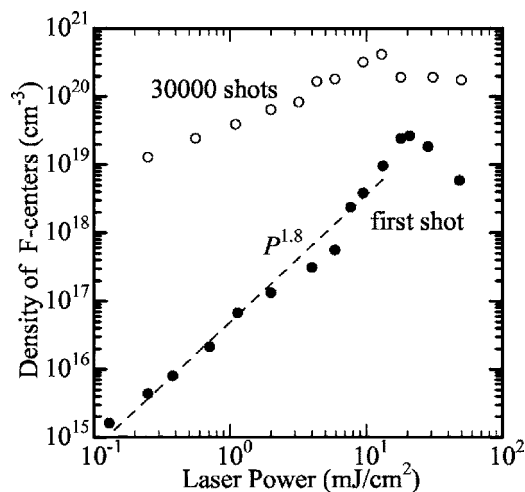
FIG. 7. The F-center density after 30 000 shots irradiation (open circles) and the first shot (closed circles) as a function of laser power. Dashed line is the best fit for the closed circles in the power region between 0.1 and ~10 mJ/cm².

nearly linearly with increasing laser power. On the other hand, the F-center density for the first shot superlinearly increases with increasing laser power P. The dependence is roughly proportional to $P^{1.8}$.

The rapid decrease of the F-center density above ~20 mJ/cm² is seen both after 30 000-shot irradiation and for the first shot. The power level of ~20 mJ/cm² can be regarded as the threshold value. As reported previously, the laser ablation is induced at the threshold power of 14 mJ/cm² at room temperature in bulk KI crystals having free surface.[47,48] The laser power of ~20 mJ/cm² is close to the threshold value of laser ablation. It should be noted that the F-absorption band cannot be observed even at 30 000 shots under the irradiation of low power below ~0.1 mJ/cm².

C. Analysis using rate equations

The F-center density depends on laser power. In order to investigate the dependence of the formation rate of the F centers under the laser power and the number of shots, the rate equations with respect to n_F and n_v are introduced, where n_F and n_v denote the densities of F center and anion vacancy at time t, respectively,[49]

$$\frac{dn_v}{dt} = k_v - k_c n_v, \qquad (3)$$

$$\frac{dn_F}{dt} = k_c n_v + k_F - k_b n_F. \qquad (4)$$

k_F and k_v are the generation rates of the F center and the anion vacancy per unit time, respectively. Since the ArF excimer laser light excites the band-to-band transition of KI, e-h pairs are initially generated by the laser excitation. When an anion vacancy captures an electron, it is converted into an F center. This conversion rate is indicated as k_c. It is generally known that the bleaching can occur through thermal and

photoinduced processes leading to direct recombination of electrons with self-trapped holes.[49] Since the laser irradiation is performed at 14 K, the thermal bleaching can be disregarded in the present case. Then, the remaining photobleaching rate of the F center is denoted as k_b. Thus, k_c and k_b are nonzero only during laser irradiation. Since k_F and k_v are also assumed to be zero without laser irradiation, n_F and n_v do not depend on time t without laser irradiation and should be kept constant. Hence, we replace the time t in Eqs. (3) and (4) with the ensemble of the discrete time duration, which denote t_i as the end time of the ith shot. The solutions for Eqs. (3) and (4) are expressed as follows:

$$n_v(t_i) = \left(n_0 - \frac{k_v}{k_c}\right)\exp(-k_c t_i) + \frac{k_v}{k_c}, \qquad (5)$$

$$n_F(t_i) = \frac{k_c n_0 - k_v}{k_b - k_c}[\exp(-k_c t_i) - \exp(-k_b t_i)]$$
$$+ \frac{k_F + k_v}{k_b}[1 - \exp(-k_b t_i)]. \qquad (6)$$

The initial conditions are set at $n_v(0) = n_0$ and $n_F(0) = 0$, where n_0 is the density of anion vacancies contained in KI crystal before laser irradiation and was estimated below 10^{16} cm⁻³ from the absorption spectrum before laser irradiation which is shown in Fig. 4. The experimental result of the F-center density as a function of the number of shot is fitted by Eq. (6) for various power levels, which are shown in Fig. 6.

In the region of the small number of shots, the linear dependence of the F-center density on laser power is observed, as seen in Fig. 6(c). From Eq. (6), it is easily understood that the F-center density at an initial stage linearly increases with the rate of $k_c n_0 + k_F$.

The fitting parameters, k_F, k_v, k_c, and k_b obtained from the fitting for 0–1000 shots are shown as a function of laser power in Figs. 8(a)–8(d). As seen in Fig. 8(a), the generation rate of the F centers k_F is proportional to 1.9th power of laser power between ~0.1 and ~20 mJ/cm², and it rapidly decreases above ~20 mJ/cm². Since the power dependence of k_F is nearly proportional to the second power of laser power, the F center is reasonably concluded to be generated through two-photon process.

As seen in Fig. 8(b), the generation rate of the anion vacancy also shows the superlinear dependence on laser power of 0.1–20 mJ/cm², while it rapidly decreases above ~20 mJ/cm². On the other hand, k_c and k_b are almost proportional to laser power between ~0.1 and 20 mJ/cm². The result indicates that the conversion of an anion vacancy into an F center and the photobleaching of the F centers occur through one-photon process, which is in good agreement with the expectation.

Under the ordinary excitation, the F-center formation simultaneously occurs with the STE formation. The studies of the femtosecond spectroscopy reveal that a common precursor state to F centers and STE is generated just after excitation. It is expected that the two-photon excitation under the high-density excitation brings the interaction between two
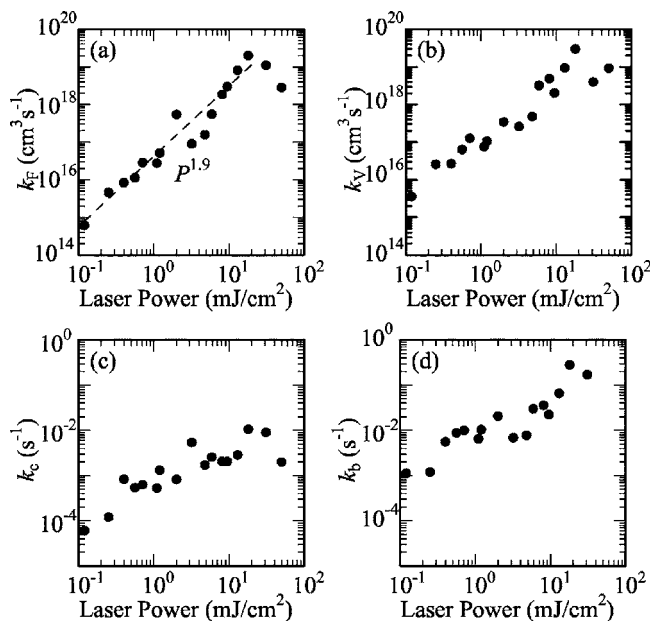
FIG. 8. The fitting parameters, k_F, k_v, k_c, and k_b, are shown as a function of the laser power. Closed circles are from the fitting results between 0 and 1000 shots. The dashed line in (a) is the best fit of k_F between 0.1 and ~20 mJ/cm².

precursor centers and the fundamental relaxation process of excitons is changed. In order to investigate the high-density effect on the exciton relaxation, we have measured the intrinsic luminescence spectra under laser irradiation for a wide range of power levels. The intrinsic luminescence spectra under the high-density excitation will give an important information about two-photon process under the irradiation of the ArF excimer laser in KI at low temperature.

IV. LASER-POWER DEPENDENCE OF INTRINSIC LUMINESCENCE

A. STE luminescence spectra

Figure 9 shows the luminescence spectra at 14 K in KI grown in the sapphire cell. As is easily noticed, the intensities of the σ and π luminescence bands increase with increasing laser power. In this measurement, the gate width of the CCD was set at 5 μs which is sufficiently longer than the decay times of both the STE luminescence bands. In the course of measurement, we have noticed that the luminescence intensity decreases slightly with increasing number of shots. Although the reason for this irradiation effect is not known yet, we have measured each luminescence spectrum within the irradiation of one to two shots for various laser powers.

In order to examine the laser-power dependence of the luminescence intensity, the luminescence spectra are decomposed into two Gaussian bands, and the integrated areas of the σ and π bands are calculated. The integrated areas of the σ and π bands, which are denoted as I_s and I_t, respectively, are plotted against laser power in Fig. 10. The power level of the ArF excimer laser varies in the range from 10^{-3} to 50 mJ/cm². The relations of $I_s \propto P^{1.0}$ and $I_t \propto P^{0.9}$
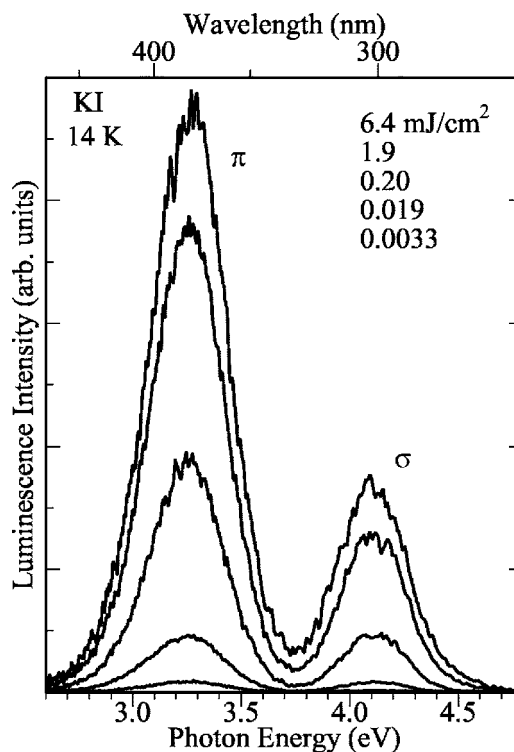
FIG. 9. Luminescence spectra due to the recombination of STEs in KI at 14 K for various laser power levels. The luminescence bands at 4.1 and 3.3 eV are denoted as the σ and π bands, respectively.

roughly hold within the power range between 10^{-3} and ~0.1 mJ/cm², where P is the laser power per unit area. These results are consistent with the results reported previously that the STE luminescence intensity increases in proportion to the excitation intensity under the ordinary excitation.[50–52] Under the irradiation in the same region of
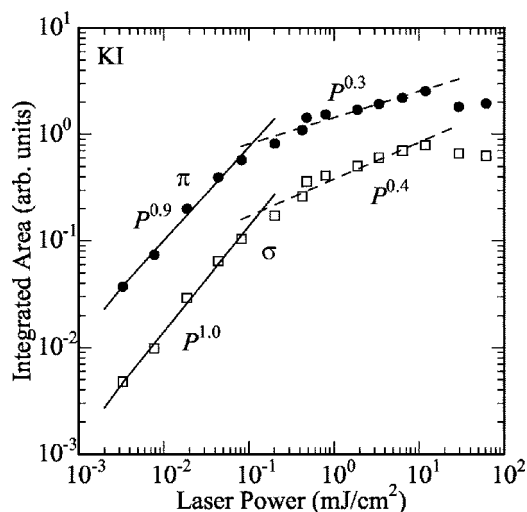
FIG. 10. Integrated area of the σ (open squares) and π (closed circles) luminescence bands as a function of laser power. Solid and dashed lines are the best fits for the experimental results of the integrated area of the σ and π bands in the regions of 10^{-3}–0.1 and 0.1–20 mJ/cm², respectively.
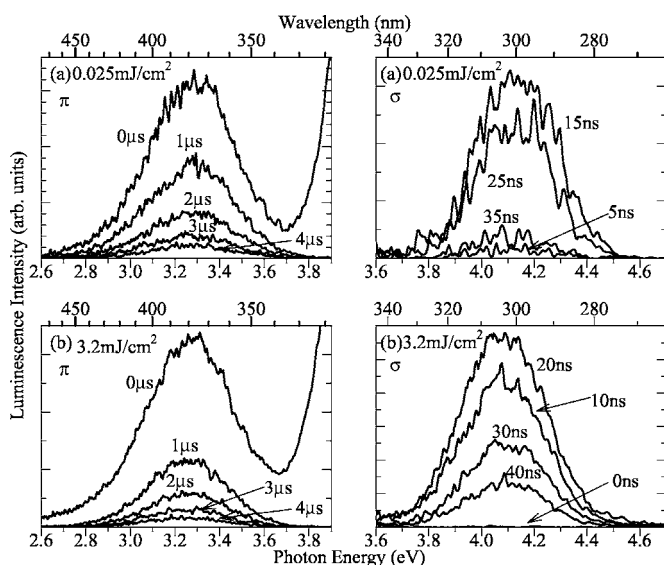
FIG. 11. Time-resolved luminescence spectra of the σ and π bands under excitation power of (a) 0.025 mJ/cm^2 and (b) 3.2 mJ/cm^2. Delay times are denoted in the figures, where the delay time at 0 is determined as the peak of the excitation laser.

power levels, the F-center formation in KI does not occur, as described in the previous section.

On the other hand, with increasing laser power, the luminescence intensity seems to be saturated. Actually, between ~ 0.1 and ~ 20 mJ/cm^2, the power dependence is roughly expressed as $I_s \propto P^{0.4}$ and $I_t \propto P^{0.3}$, as seen in Fig. 10. The reduction of luminescence efficiency above ~ 0.1 mJ/cm^2 suggests two possibilities: the appearance of an extra luminescence band in addition to the ordinary STE luminescence and the change from exciton relaxation process occurring under the weak excitation.

According to the previous study in RbI, an extra luminescence band is observed in the time-resolved spectra under dense excitation in addition to the ordinary STE luminescence.[33] With the appearance of the extra luminescence band, the saturation of the π luminescence intensity is simultaneously observed. In the present study of KI, the extra luminescence and the decay processes of the σ and π bands have been investigated. The time-resolved luminescence spectra and the decay profiles will be stated in the latter.

Above ~ 20 mJ/cm^2, I_s and I_t rapidly decrease. The similar behavior above ~ 20 mJ/cm^2 has been observed in the F-center density for 30 000 shots, which are shown in Fig. 7. The power level of ~ 20 mJ/cm^2 can be regarded as a kind of threshold value. Since the value is close to the threshold value of laser ablation, rapid decrease of efficiencies of both the STE luminescence and the F-center formation observed above ~ 20 mJ/cm^2 are considered to have a close relation with laser ablation.

In order to investigate the extra luminescence in KI under the high-density excitation, the time-resolved luminescence spectra were measured at 14 K. The spectra under the weak and high excitations of 0.025 and 3.2 mJ/cm^2 are shown in Figs. 11(a) and 11(b), respectively. The decay time of the σ band mainly observed is known to be ~ 2 ns.[53] The gate

width to detect the σ luminescence band was set at 7 ns because the minimum gate width of the CCD is limited at 7 ns. On the other hand, the decay time of the π band mainly observed is known to be ~ 2 μs. The gate width to detect the π luminescence was set at 50 ns.

Since the decay time of the σ band is much shorter than that of the π band, the low-energy tail of the σ band is seen above 3.7 eV in the π band at 0 μs, which is shown in the left side of Figs. 11(a) and 11(b). Though the time-resolved luminescence spectra of the π band for the delay times between 0 and 1 μs are not shown in Fig. 11, we also measured the time-resolved spectra in the time range in detail. It was confirmed that any other luminescence band was not observed in this range.

The peak positions of both σ and π bands at 3.2 mJ/cm^2 slightly shift to the lower-energy side than those at 0.025 mJ/cm^2. The low-energy shift of the STE bands does not arise from the temperature rise due to the intense laser light because the peak position shifts to the high-energy side with increasing temperature.[54] Then, one may consider that the low-energy shift arises from the appearance of the extra luminescence band. However, this peak shift is much smaller than the bandwidth. In fact, the spectral shapes of both σ and π bands are essentially unchanged with increasing delay time. Thus, it is concluded that this peak shift does not arise from the appearance of the extra band, although the reason is not clear yet. In KI, the extra luminescence does not appear even under the high-density excitation in the different way from RbI. The absence of the extra luminescence in KI under the high-density excitation would be caused by the difference of STE relaxation between RbI and KI.[55]

As a result, we propose that the reduction of luminescence efficiency above ~ 0.1 mJ/cm^2 arises from the change of exciton relaxation process due to the high-density excitation. With the reduction of luminescence efficiency, the F-center formation arising from the two-photon process is simultaneously observed above ~ 0.1 mJ/cm^2. Thus, the change of exciton relaxation proposed here is also attributed to the two-photon process. In the next section, we will present the effect of two-photon process on the decay profiles of the STE luminescence.

B. Decay profiles of STE luminescence

The σ band in KI is known to be composed of fast-decaying and slowly decaying components with the decay times of 2.1 ns and 2 μs at 12.4 K, respectively.[53] The fast-decaying and slowly decaying components are attributed to a singlet STE state and a nearly degenerate singlet-triplet STE state, respectively. The time-integrated intensity of the slowly decaying component is particularly low and is only 4% of the total intensity.

The π band in KI is known to be composed of fast-decaying and slowly decaying components with the decay times of 180 ns and 2 μs at 14 K, respectively.[56] The fast-decaying component arises from one of the triplet sublevels of STE, which can be observed only below 20 K.

We measured the decay profile of the luminescence intensity at a peak position from the time-resolved luminescence
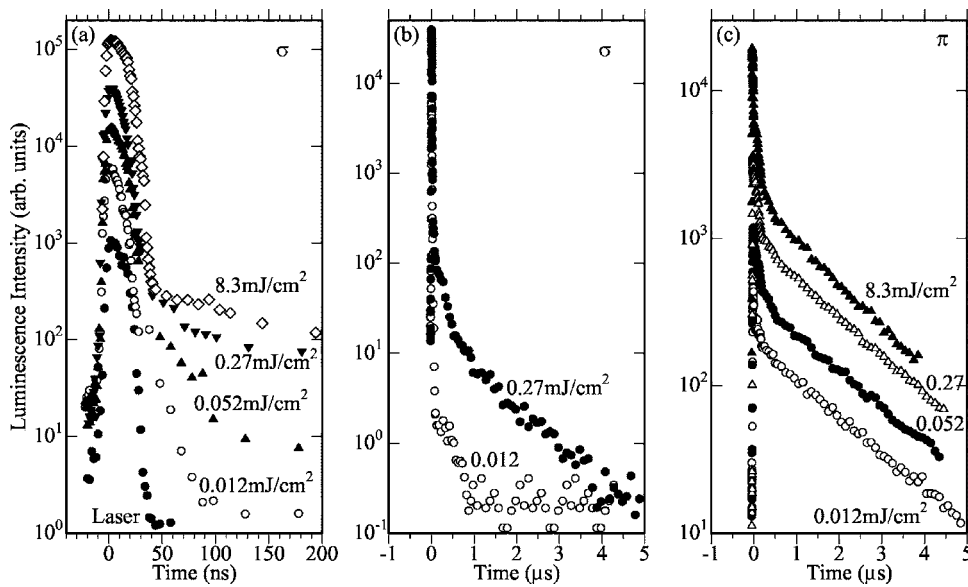
FIG. 12. (a) Decay curves, (b) the σ band at 4.1 eV, and (c) the π band at 3.3 eV under excitation with various levels of the laser power. The time profile of the exciting laser pulse is also shown by the closed circles in (a).

spectra for various delay times at 14 K. The decay profiles are shown in Figs. 12(a)–12(c). In the course of measurement, we have noticed that the luminescence intensity gradually decreases until ~1000 shots above ~0.1 mJ/cm² and seems to be constant after then. In such cases, we measured the decay curves practically after the irradiation of 1000 shots.

1. σ luminescence

The decay profiles for the σ band at the peak of 4.1 eV under the excitation for various levels of the laser power are shown in Figs. 12(a) and 12(b). The fast component which resembles the excitation laser profile is observed at the delay times between −10 and 30 ns. The fast-decaying component of the σ luminescence is known to have the decay constant of ~2 ns which is much shorter than the duration of the ArF excimer laser of 15 ns. Thus, it is reasonable that the decay curve of the fast component agrees with that of the laser profile. The slowly decaying component of ~2 μs cannot be observed under the weak excitation. With increasing laser power, a slow component clearly increases, as shown in Fig. 12(b).

In order to determine the time constant and the relative intensity of each decay component in the σ decay profiles, a decay curve is decomposed into several exponential functions. Figure 13(a) shows the experimental data (open circles) and a single exponential fit (dotted line) which is determined by the analysis considering the pulse duration of the ArF excimer laser (15 ns). This analysis has been generally used, when the decay time is shorter than the duration of excitation pulse. In the present study, the decay times shorter than ~100 ns are determined by means of this analysis. The decay time of the fastest component seen in Fig. 13(a) is determined to be about 1 ns.

Under the high excitation levels of 1.1 and 5.7 mJ/cm², the slow component becomes clear, as seen in Figs. 13(b) and 13(c), respectively. At first, the decay time of the slowest component is determined to be 630 ns at 1.1 mJ/cm² and 620 ns at 5.7 mJ/cm². The decay times of the slowly decay-

ing components under the high excitation are quite different from that of the nearly degenerate singlet-triplet STE (2 μs). Next, we plot the experimental data subtracted by the slowest component, which are denoted by closed circles in Figs. 13(b) and 13(c). At 1.1 mJ/cm², the subtracted data can be fitted to a sum of two exponentially decaying components. The successive analysis, as described above, gives two fast-decaying components of 90 ns (solid line) and 2 ns. At 5.7 mJ/cm², on the other hand, the subtracted data can be fitted to a sum of three exponentially decaying components. The decay constants are determined to be 110 ns (solid line), 20 ns (dash-dotted line), and 4 ns.

For the range of the laser power between 10^{-3} and 50 mJ/cm², we perform the similar analysis. In Fig. 14, the decay times are plotted against laser power. In all regions examined, the fastest component with the decay time of 1–4 ns, denoted as S, is always present. In addition, ~600 and ~100 ns decay components appear above ~0.1 mJ/cm², and an ~10 ns component comes out above ~2 mJ/cm². We denote these decay components as A, B, and X, respectively.

The fastest component S with the time constant of 1–4 ns is observed in the present experiment. Since the value is close to the fast-decaying component of ~2 ns at 12.4 K,[53] S is attributed to the radiative decay of the singlet STEs. The decay components of the σ band with the decay times of A~600 ns, B~100 ns, and X~10 ns have not been reported in the σ luminescence band so far. The decay components of A and B appear above ~0.1 mJ/cm². As described in the previous section, the two-photon process becomes effective above ~0.1 mJ/cm² and the change of exciton relaxation process is considered to occur. Since the decay components of A and B are observed only above ~0.1 mJ/cm², the appearance of A and B would arise from exciton relaxation process due to the two-photon process. The decay component of X become observable above ~2 mJ/cm².

A, B, and X do not arise from the temperature increase under strong laser light irradiation because the decay times of A, B, and X remain almost constant with increasing laser
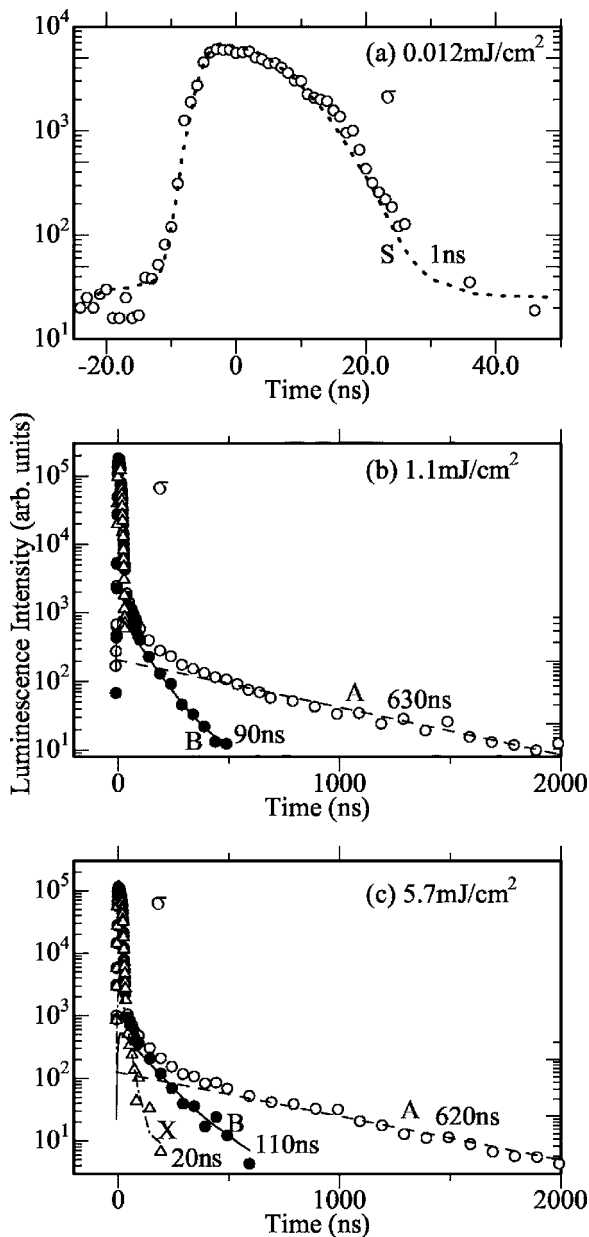
FIG. 13. Decay curves of the σ luminescence band under excitation with (a) 0.012 mJ/cm^2, (b) 1.1 mJ/cm^2, and (c) 5.7 mJ/cm^2. Open circles are the experimental results. Closed circles are the experimental data subtracted by the slowest component which is indicated by dash lines. The fastest-decaying component is indicated by dotted line in (a). The decay constants are shown on the decomposed decay curves.

power. If the temperature increases, the decay constant has to change with increasing laser power. Thus, the appearance of A and B strongly suggests that some quasistable states related with the STE relaxation newly appears under the high-density excitation. The new quasistable state will be discussed later.

The time-integrated intensities for the decay components of S, A, B, and X are plotted as a function of laser power in Fig. 15. The time-integrated intensity for S is proportional to laser power between 10^{-3} and $\sim$0.1 mJ/cm^2, and it seems to saturate above $\sim$0.1 mJ/cm^2. The intensity for S between
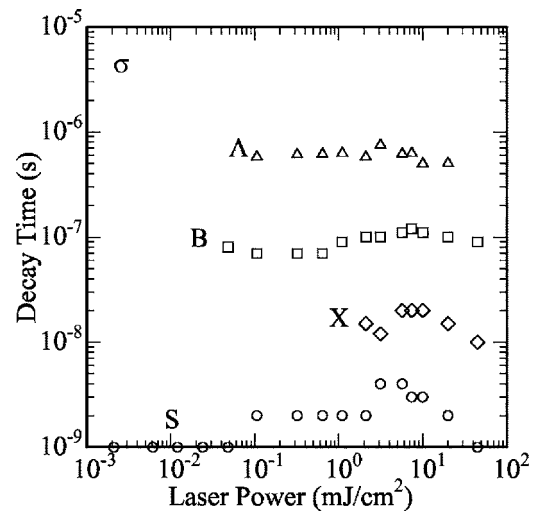
FIG. 14. Decay constants of the σ luminescence band as a function of laser power. Open circles, triangles, squares, and rhombuses show the decay components of S, A, B, and X, respectively.

$\sim$0.1 and $\sim$2 mJ/cm^2 roughly follows the 0.4th power of laser power. Such power dependence is also observed in the experimental result of the integrated area of the σ band shown in Fig. 10. In this region of power levels, the intensities for A and B roughly follow the 0.4th and 0.8th powers of laser power, respectively. The laser power dependence of the time-integrated intensities for A and B would arise from exciton relaxation process due to the two-photon process.

The intensity for X observed above $\sim$2 mJ/cm^2 does not depend on laser power. The intensities for A and B are also independent of laser power above $\sim$2 mJ/cm^2. This peculiar power dependence above $\sim$2 mJ/cm^2 as well as the origin of X remains an open question.
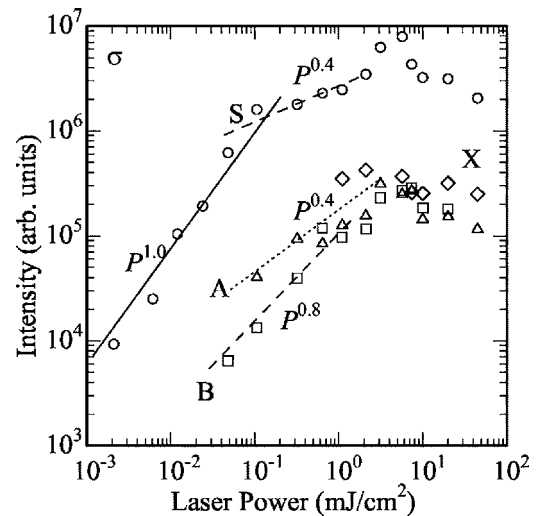
FIG. 15. Laser-power dependence of the time-integrated intensities of the decay components of S, A, B, and X. Open circles, triangles, squares, and rhombuses indicat the time-integrated intensities of S, A, B, and X, respectively. Solid line is the best fit between 10^{-3} and $\sim$0.1 mJ/cm^2. Dashed and dotted lines are the best fits between $\sim$0.1 and $\sim$2 mJ/cm^2.

2. π luminescence

The decay curves for the π band at the peak of 3.3 eV under the excitation for various levels of laser power are shown in Fig. 12(c). It is easily noted that the slowly decaying component of about 2 μs is dominant for all the excitation power levels. The fast-decaying component is barely visible under the weak excitation with the laser power of 0.012 mJ/cm², while its relative intensity becomes larger with increasing power levels.

In order to determine the time constant and relative intensity of each decay component, a decay curve is decomposed into several exponential functions. At first, the time constants τ_t of the slowest components are determined to be 1.8 μs at 0.012 mJ/cm², 1.7 μs at 1.1 mJ/cm², and 1.6 μs at 5.7 mJ/cm², respectively, as shown in Figs. 16(a)–16(c). We also plot the experimental data subtracted by the slowest component (dash line). It is clear that the fast component is well expressed by a single exponential decay with a time constant of 120 ns at 0.012 mJ/cm², as shown in Fig. 16(a). At 1.1 mJ/cm², the subtracted data cannot be fitted to a single exponential function. The data can be expressed by a sum of two exponential functions, as shown in Fig. 16(b). The successive analysis, as described above, gives the time constant for the longer decay component (dotted line) as 520 ns, while that for the shorter one (solid line) as 80 ns. At 5.7 mJ/cm², the subtracted data can be expressed by a sum of three exponential functions, as shown in Fig. 16(c), the decay constants of which are determined to be 470 ns (dotted line), 110 ns (solid line), and 15 ns (dash-dotted line).

Within the range of the laser power between 10^{-3} and 50 mJ/cm², we perform the similar analysis and plot the decay constants as a function of laser power, which is shown in Fig. 17. In all the regions examined, two components with the decay times of ∼2 μs and ∼100 ns, denoted as T and T′, are always present. The time constant of ∼2 μs is in agreement with the decay time of the slowly decaying component of the π band.[56] On the other hand, the decay component with the time constant of ∼100 ns is close to that of the fast-decaying component of the π band. The decay component of T′ is attributed to the radiative decay of the triplet sublevel of the fast-decaying component of the π band.

In addition, an ∼500 ns decay component appears above ∼0.1 mJ/cm², and an ∼10 ns component comes out above ∼2 mJ/cm². The decay components have not been reported in the π band. One may notice that the ∼500 and ∼10 ns components have very close values to the decay constants of A and X observed in the σ band, respectively. In both σ and π bands, the ∼500 ns decay component appears above ∼0.1 mJ/cm², and the ∼10 ns decay component appears above ∼2 mJ/cm². This agreement indicates that the decay components of A and X observed in the σ band have the same origins as those observed in the π band, respectively. Then, we denote the ∼500 and ∼10 ns decay components observed in π band as A and X, respectively. In the π band, the decay component corresponding to B observed above ∼0.1 mJ/cm² in the σ band may overlap with the decay component of T′.

Figure 18 shows the time-integrated intensity for each decay component of T, T′, A, and X as a function of laser
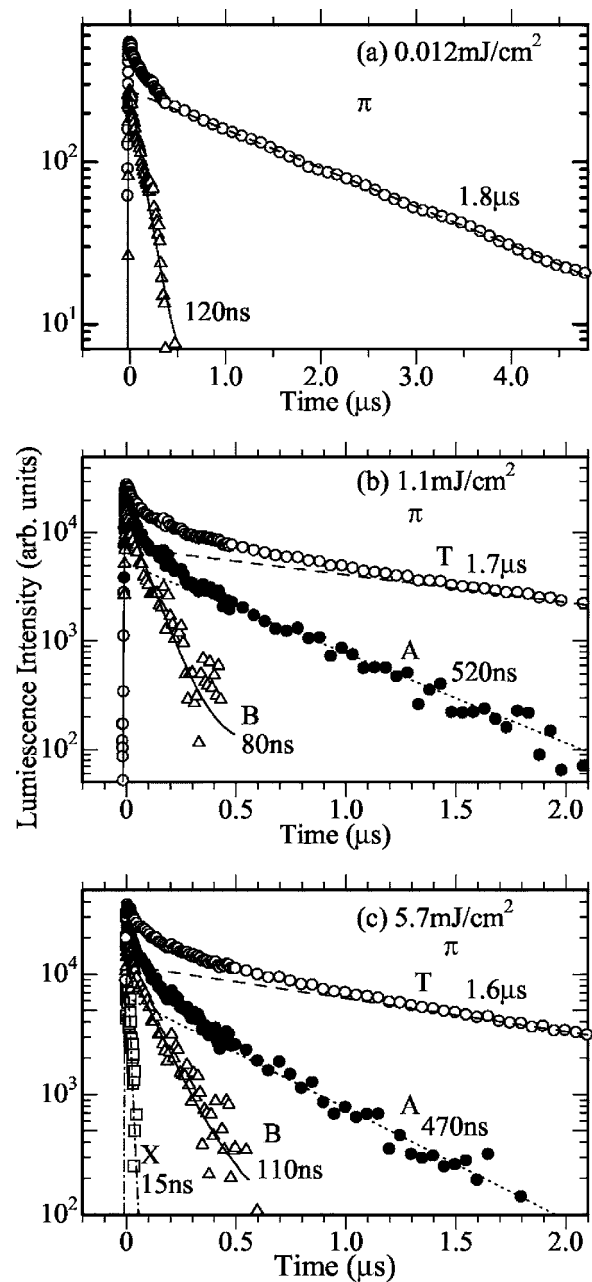
FIG. 16. Decay curves of the π luminescence band under excitation with (a) 0.012 mJ/cm², (b) 1.1 mJ/cm², and (c) 5.7 mJ/cm². Open circles are the experimental results. Closed circles are the experimental data subtracted by the slowest component which is indicated by dashed lines. The decay constants are shown on the decomposed decay curves.

power. The time-integrated intensities for T and T′ is roughly proportional to laser power between 10^{-3} and 0.1 mJ/cm², and they seem to saturate above ∼0.1 mJ/cm². The intensity for T between ∼0.1 and ∼2 mJ/cm² roughly depends on the 0.4th power of laser power. Such power dependence is also observed in the experimental result of the integrated area of the π band shown in Fig. 10. In this region of power levels, the intensities for A and T′ roughly depend on the 0.8th and 0.6th powers of laser power, respectively. The laser-power dependence of the time-integrated intensi-
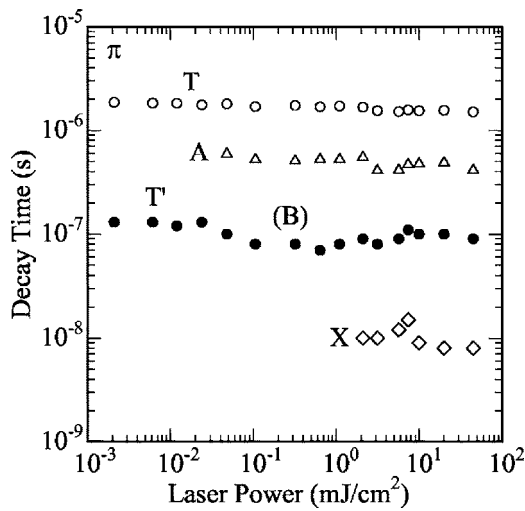
FIG. 17. Decay times of the π luminescence at 14 K as a function of laser power. Open and closed circles show the decay components of T and T′, respectively. Open triangles and rhombuses show the decay components of A and X, respectively. Closed circles shown above ~0.1 mJ/cm² are indicated as (B).

ties for A and T′ would arise from exciton relaxation process due to the two-photon process because the decay components of A and T′ are observed above ~0.1 mJ/cm². Above ~2 mJ/cm², the intensities for A, X, and T′ remain almost constant with increasing laser power. Such behavior is similar to the power dependence of the time-integrated relative intensity of the σ band.

C. FE and biexciton luminescence

Under the excitation of the intrinsic absorption region at low temperatures, only alkali iodide crystals exhibit the FE
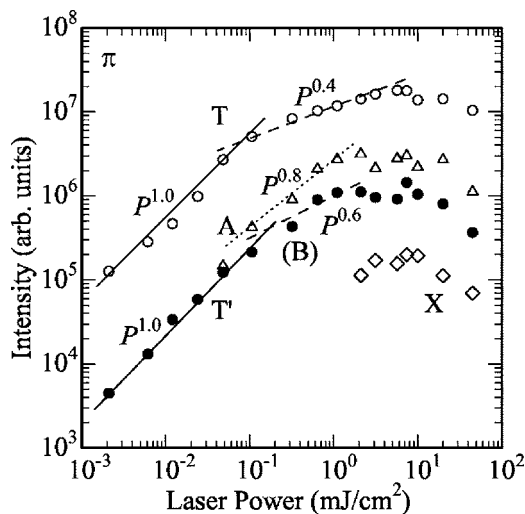
FIG. 18. Laser-power dependence of the time-integrated intensities of the decay components having time constants of T, T′, A, and B. Open and closed circles are denoted as T and T′, respectively. Open triangles and open rhombuses are indicated as A and X, respectively. Solid lines are the best fits between 10^{-3} and 0.1 mJ/cm². Dashed and dotted lines are the best fits between ~0.05 and ~1 mJ/cm². Closed circles shown above ~0.1 mJ/cm² are indicated as (B).
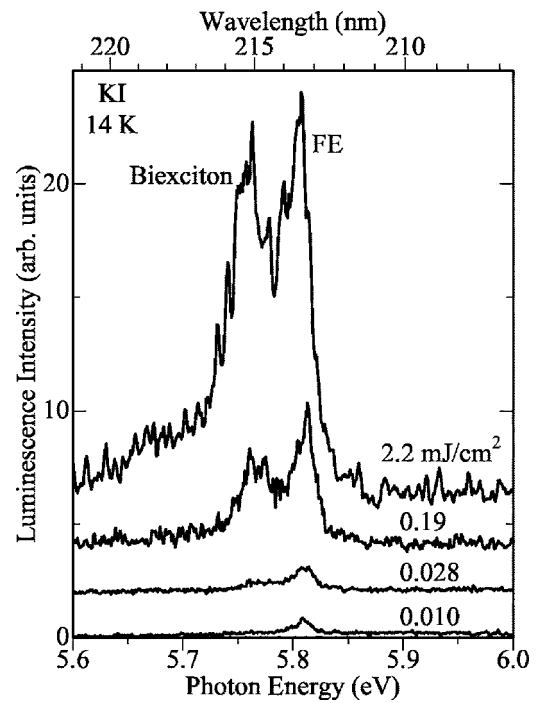
FIG. 19. Luminescence spectra of the recombination of an FE and a biexciton leaving an exciton behind. Laser powers are denoted in the figure.

luminescence in the band-edge region.[35,37,38,50–52,57] The peak position of the FE luminescence is known to be ~5.83 eV in the bulk KI crystal at 14 K.[51] Under the high-density excitation, the biexciton luminescence is observed in addition to the FE luminescence. The peak position of the biexciton luminescence is slightly lower than that of the FE luminescence. In KI, the peak position of the biexciton luminescence is 5.78 eV at 10 K.[51]

Figure 19 shows the luminescence spectra of KI in the band-edge region under the irradiation of the ArF excimer laser at 14 K. The luminescence band peaking at 5.81 eV is due to the FE, which slightly depends on samples. The luminescence band at 5.76 eV observed above ~0.028 mJ/cm² is the biexciton one. As is easily noticed, the intensities of the FE and biexciton bands increase with increasing laser power.

By the way, the peak position of the FE band observed in the present study is lower by about 0.02 eV than that observed in the bulk KI crystal. The lower-energy shift is attributed to the dilatational strain acting on the thin crystal grown from melt in the small gap of a cell. According to the study previously reported,[58] the peak position of the FE luminescence shifts to the low-energy side with decreasing thickness of the thin crystal because the dilatational strain becomes larger. The thickness of the present crystal is about 10 μm. The FE luminescence peak in the thin crystal of 10 μm thickness is 5.82 eV at 11 K,[59] whose value is almost in good agreement with the peak energy of the FE luminescence observed in the present study.

In order to examine the laser-power dependence of luminescence intensity, a luminescence spectrum is decomposed into two or three Lorentzian bands, and the integrated areas of each band are calculated. The integrated areas of the FE
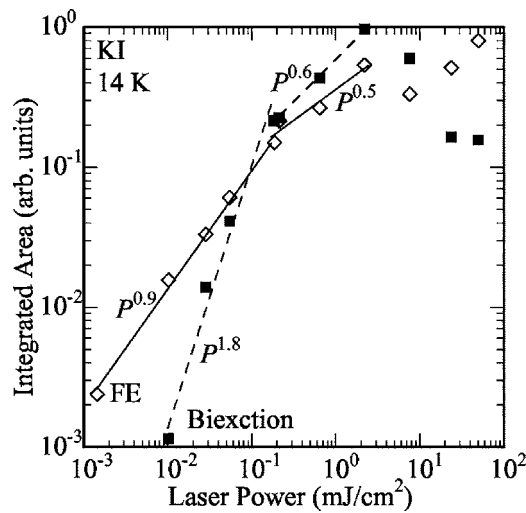
FIG. 20. Integrated area of the FE and biexciton luminescence bands as a function of laser power. Open and closed rhombuses indicate the integrated areas of the FE and biexciton luminescence bands, respectively. Solid and broken lines are best fits for the FE and biexciton luminescence bands, respectively. The slopes of both lines change in the border of the power level of ~ 0.1 mJ/cm^2.

and biexciton bands, which are denoted as I_e and I_b, respectively, are plotted against laser power in Fig. 20. It is found that the relations of $I_e \propto P^{0.9}$ between 10^{-3} and ~ 0.1 mJ/cm^2 and $I_b \propto P^{1.8}$ between ~ 0.01 and ~ 0.1 mJ/cm^2 roughly hold. I_b quadratically depends on I_e. This result is a typical nature of the intensities of the FE and biexciton luminescence.

As the laser power increases from ~ 0.1 mJ/cm^2, the luminescence intensity seems to be saturated. Actually, between ~ 0.1 and ~ 2 mJ/cm^2, the power dependence is roughly expressed as $I_e \propto P^{0.5}$ and $I_b \propto P^{0.6}$. The saturation behavior of the luminescence intensities above ~ 0.1 mJ/cm^2 is also observed in the laser-power dependence of the STE luminescence intensity. It should be noted here that the luminescence intensity of biexciton is larger than that of FE between ~ 0.1 and ~ 2 mJ/cm^2. According to a previous study on biexcitons,[50,51] the luminescence intensity of biexciton never exceeds that of FE under the excitation of $n=1$ exciton absorption region. The exceeding increase of the biexciton luminescence above ~ 0.1 mJ/cm^2 indicates that the two-photon process effectively governs the exciton relaxation. However, the FE and biexciton luminescence intensities are much smaller than the STE luminescence intensity. Therefore, the existence of the biexciton luminescence would not have any effect on the *F*-center formation in the present case. In addition, it has been reported that the relaxation of the biexciton does not lead to the *F*-center formation.

Above ~ 2 mJ/cm^2, with increasing laser power, the luminescence intensity of the FE seems to be independent of laser power and that of the biexciton decreases rapidly. The FE luminescence is very sensitive to impurities and defect centers contained in the crystal. It is known that the *F* centers of 10^{17} cm^{-3} quench the FE luminescence band almost completely.[60] Above ~ 2 mJ/cm^2, the *F*-center density for the first shot exceeds 10^{17} cm^{-3}, as seen in Fig. 6(c). How-

ever, the FE luminescence band can be observed above ~ 2 mJ/cm^2. This result may be ascribed to the extremely high-density excitation.

V. DISCUSSION

A. Existence of precursor state

We have investigated the *F*-center formation in KI at 14 K. The creation of the *F* centers is verified under the irradiation of the ArF excimer laser with the power level above ~ 0.1 mJ/cm^2. From the analysis using the rate equations, it is found that the generation rate of the *F* center is nearly in proportion to the second power of the laser power between ~ 0.1 and ~ 20 mJ/cm^2. Thus, the *F*-center formation in the present case is concluded to result from the two-photon process. This fact indicates that the discussion based on the thermal conversion mechanism from the triplet STE to the *F* center is useless. According to the recent study of the femtosecond spectroscopy, a precursor state, which is common to both *F* center and STE, is generated just after the excitation and decays within ~ 10 ps.[19] Thus, it is reasonable to discuss the present experimental result on the basis of the *F*-center formation via the precursor state. Here, we assume that the *F*-center formation results from the interaction between two precursor states (paired precursors) excited by two-photon process.

The two-photon excitation usually occurs in the following two stages. The first excitation creates one precursor state leading to the STE state through the subsequent relaxation. In the second stage of two-photon excitation, the precursor or STE state is photoexcited at the neighboring site of the precursor or STE state generated by the first excitation. This assumption does not exclude the coherent two-photon excitation to the paired precursor state. However, the phase relaxation rate is very fast as compared with the relaxation rate of the precursor or STE state. Further, since the pulse duration of the ArF excimer laser (15 ns) is much longer than the decay time of the precursor state (~ 10 ps), the second excitation to the paired precursor state will mainly occur after the relaxation to the STE state.

It is expected that the presence of the paired precursor state under the high density changes the fundamental relaxation process of excitons observed under the ordinary excitation. The change may appear in the STE luminescence spectra. Although there is no direct experimental evidence concerning the presence of the paired precursors or STEs, the indirect experimental evidence can be seen in the experimental results of the STE luminescence spectra under the excitation between 10^{-3} and 50 mJ/cm^2.

Between 10^{-3} and ~ 0.1 mJ/cm^2, the luminescence intensity of the STE increases in proportion to the excitation intensity. This result is consistent with the data under the ordinary excitation condition. The decay times of the STE luminescence bands are also consistent with those reported previously.[53,56] Above ~ 0.1 mJ/cm^2 which corresponds to the laser power occuring two-photon process, the luminescence efficiency decreased and the additional decay components are newly observed. The additional decay components exhibit no change of the decay time constants even under the
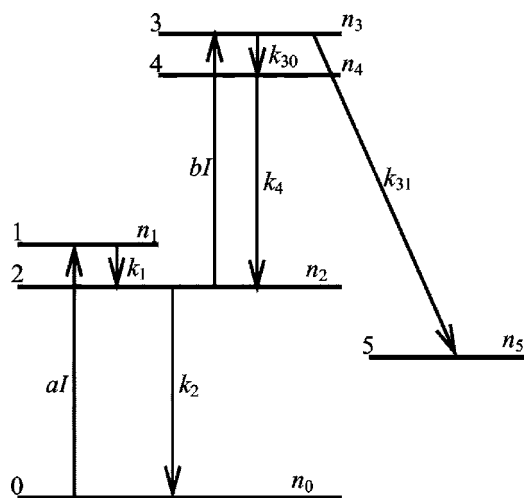
FIG. 21. Schematic illustration of energy levels involving two-photon process.

condition of the increase of the laser power. This fact strongly suggests that some quasistable states newly appear through the two-photon process. The paired STE state, which is the relaxation state of the paired precursor state, is the most probable candidate for that. The paired STE state will cause the reduction of the luminescence efficiency and the appearance of the new decay components. As a result, they relate to the F-center formation. In the following, we will discuss the microscopic mechanisms for these phenomena in a unified way.

B. Analysis using rate equations involving two-photon process

We try to simulate qualitatively the present experimental results by using a simple model involving two-photon excitation process, as described above. A simple rate equation model introduced here does not distinguish the singlet and triplet states of the STEs. The energy levels involving two-photon process are schematically illustrated in Fig. 21. The first excitation brings the transition from the ground state denoted as 0 to the precursor state denoted as 1 and the subsequent relaxation causes the population on the STE state denoted as 2. The populations at their energy levels are denoted as n_0, n_1, and n_2, respectively. The excitation rate from 0 to 1 is denoted by aI, where I is the excitation intensity. The decay rate from precursor state 1 to STE state 2 is indicated by k_1. Since the decay time of the precursor state is generally known to be within ~ 10 ps,[19] k_1^{-1} is considered to be about 10 ps. The decay rate from STE state 2 to ground state 0 is indicated by k_2, which corresponds to the decay rate of the STE luminescence.

The second excitation to the paired precursor state occurs after the relaxation from 1 to 2. Thus, the two-photon excitation only occurs via the process 0-1-2-3, where 3 denotes the paired precursor state. The excitation rate from 2 to 3 is denoted as bI and the population of the state 3 is denoted as n_3.

The generation of the F center occurs through the relaxation from state 3. Therefore, there are two relaxation path-

ways from state 3. One is to state 4 with the decay rate of k_{30} and the other is to state 5 with the decay rate of k_{31}, where states 4 and 5 denote the paired STE state and the F-center state, respectively, and their populations are denoted as n_4 and n_5. The radiative decay rate from 4 to 2 is denoted as k_4. Since no additional luminescence band is observed even under the high-density excitation, it is reasonable that the energy difference between 4 and 2 states is supposed to be nearly the same as that between 2 and 0 states.

On the basis of the simple model, as described above, the populations n_i ($i=1-5$) are governed by the following rate equations:

$$\frac{dn_1}{dt} = aIn_0 - k_1n_1, \tag{7}$$

$$\frac{dn_2}{dt} = k_1n_1 - k_2n_2 - bIn_2 + k_4n_4, \tag{8}$$

$$\frac{dn_3}{dt} = bIn_2 - k_{30}n_3 - k_{31}n_3, \tag{9}$$

$$\frac{dn_4}{dt} = k_{30}n_3 - k_4n_4, \tag{10}$$

$$\frac{dn_5}{dt} = k_{31}n_3, \tag{11}$$

where we neglect the ground-state reduction during the excitation. Since the relaxation times of k_1^{-1} and $1/(k_{30}+k_{31})$ are expected to be within about 10 ps which is much shorter than the pulse duration of the ArF excimer laser, the quasistationary conditions hold for states 1 and 3: $dn_1/dt \approx 0$ and $dn_3/dt \approx 0$. Then, Eqs. (7) and (9) become

$$n_1(t) = \frac{aI}{k_1}n_0, \tag{12}$$

$$n_3(t) = \frac{bI}{k_{30}+k_{31}}n_2(t). \tag{13}$$

In addition, within the pulse duration of the ArF excimer laser ($0 \leq t \leq t_w$), for simplicity, the excitation intensity I is assumed to be constant, where t_w is the pulse duration. Then, the solutions of Eqs. (8), (10), and (11) are considered as follows. In order to distinguish the solution during laser irradiation ($0 \leq t \leq t_w$) and after irradiation ($t_w \leq t$), n_i is replaced with N_i ($i=2, 4$, and 5) during laser irradiation.

$$N_2(t) = \frac{an_0I}{2\sqrt{r}}\left[\frac{k_4-k_2-bI+\sqrt{r}}{l_1}(e^{l_1t}-1)\right.$$
$$\left. - \frac{k_4-k_2-bI-\sqrt{r}}{l_2}(e^{l_2t}-1)\right], \tag{14}$$

$$N_4(t) = \frac{abn_0I^2}{\sqrt{r}}\frac{k_{30}}{k_{30}+k_{31}}\left(\frac{e^{l_1t}-1}{l_1} - \frac{e^{l_2t}-1}{l_2}\right), \tag{15}$$

$$N_5(t) = \frac{abn_0I^2}{2\sqrt{r}} \frac{k_{31}}{k_{30} + k_{31}} \left[\frac{k_4 - k_2 - bI + \sqrt{r}}{l_1} \left(\frac{e^{l_1 t} - 1}{l_1} - 1 \right) \right.$$
$$\left. - \frac{k_4 - k_2 - bI - \sqrt{r}}{l_2} \left(\frac{e^{l_2 t} - 1}{l_2} - t \right) \right],$$

(16)

where l_1, l_2, and r are given as

$$l_1 = -\frac{k_2 + k_4 + bI}{2} + \frac{\sqrt{r}}{2},$$

(17)

$$l_2 = -\frac{k_2 + k_4 + bI}{2} - \frac{\sqrt{r}}{2},$$

(18)

$$r = (k_4 - k_2 - bI)^2 + 4k_4 \frac{k_{30}}{k_{30} + k_{31}} bI.$$

(19)

After the laser irradiation ($t_w \leqslant t$), the excitation intensity I becomes 0 ($I = 0$). Then, Eqs. (8), (10), and (11) become

$$n_2(t) = \frac{k_4}{k_2 - k_4} n_{40} e^{-k_4(t-t_w)} + \left(n_{20} - \frac{k_4}{k_2 - k_4} n_{40} \right) e^{-k_2(t-t_w)},$$

(20)

$$n_4(t) = n_{40} e^{-k_4(t-t_w)},$$

(21)

$$n_5(t) = n_{50},$$

(22)

where n_{20}, n_{40}, and n_{50} are the populations of 2, 4, and 5 at the end of the laser irradiation and correspond to $N_2(t_w)$, $N_4(t_w)$, and $N_5(t_w)$, respectively.

From Eqs. (20) and (21), the STE luminescence intensity $I_j(t) (j = s, t)$ is calculated as follows:

$$I_j(t) = k_2 n_2(t) + k_4 n_4(t)$$
$$= \frac{k_4(2k_2 - k_4)}{k_2 - k_4} n_{40} e^{-k_4(t-t_w)}$$
$$+ k_2 \left(n_{20} - \frac{k_4}{k_2 - k_4} n_{40} \right) e^{-k_2(t-t_w)},$$

(23)

where I_s and I_t represent the σ and π luminescence, respectively, and we choose the parameters separately for each luminescence process.

It is noted here that two decay components expressed by the decay rates k_2 and k_4 appear in $I_j(t)$. Since k_2^{-1} corresponds to the decay constant of the ordinary STE luminescence, the additional decay component of k_4^{-1} is attributed to the relaxation from the paired STEs to a single STE. Thus, the present model succeeds to explain qualitatively the appearance of the additional decay component in the STE luminescence. However, it does not explain the presence of two additional decay components with the time constants of ~100 and ~500 ns observed both in σ and π luminescence bands. This is because a too simplified model is employed. Under the high-density excitation, various excitation and relaxation processes which include coherent and incoherent excitation processes would occur. The expressions using the rate equations are difficult to fully explain these processes. In
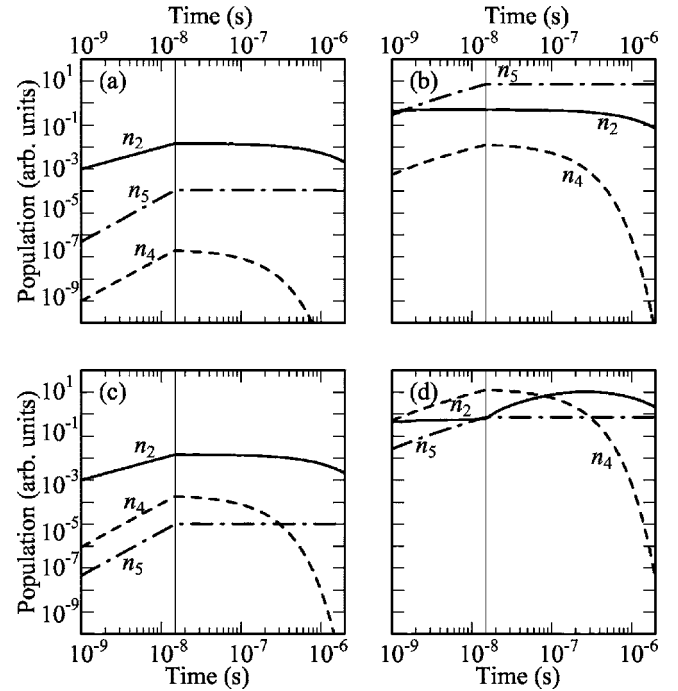
FIG. 22. Populations of n_2, n_4, and n_5 in the case of the π luminescence. (a) and (c) of the left side of these figures show the simulations under weak excitation, while (b) and (d) of the right side under the high density excitation. (a) and (b) are in the case of $k_{30}:k_{31} = 1:1000$ and (c) and (d) are of 10:1. Solid, dashed, and dash-dotted lines denote n_2, n_4, and n_5, respectively. The thin solid lines perpendicularly drawn at 15 ns indicate the pulse duration of the ArF excimer laser. Both vertical and horizontal axes take a logarithmic scale.

the present case, we have employed a simple relaxation process to account for the essential part of the F-center formation and the nonlinear dependence of the luminescence on the excitation laser power. The next section shows the simulations with the application of appropriate parameters to the solutions of the rate equations [Eqs. (17)–(22)].

C. Simulation

We have simulated the cases for weak and strong excitations, where the excitation intensity I takes a value of 10^6 and 10^9 cm^{-2} s^{-1} for the weak and strong excitations, respectively. The values of k_i ($i = 2$, 3, and 4) are determined as follows. In the σ luminescence, the ordinary decay time k_2^{-1} is determined to be 1 ns, while in the π luminescence, it is determined to be 1 μs. The ratio of k_{30} and k_{31} is treated as a parameter. Although the decay time of the additional decay component k_4^{-1} can be taken as either 100 or 500 ns, we choose 100 ns here as k_4^{-1}. The simple model described in the foregoing section is suitable for both the σ and π STEs. We mainly present the simulated results of the π luminescence in this section.

At first, the time progress of the populations at the energy levels of 2, 4, and 5 is simulated. The results of the simulations in case of the π luminescence are shown in Figs. 22(a)–22(d). All the populations, n_2, n_4, and n_5, increase dur-
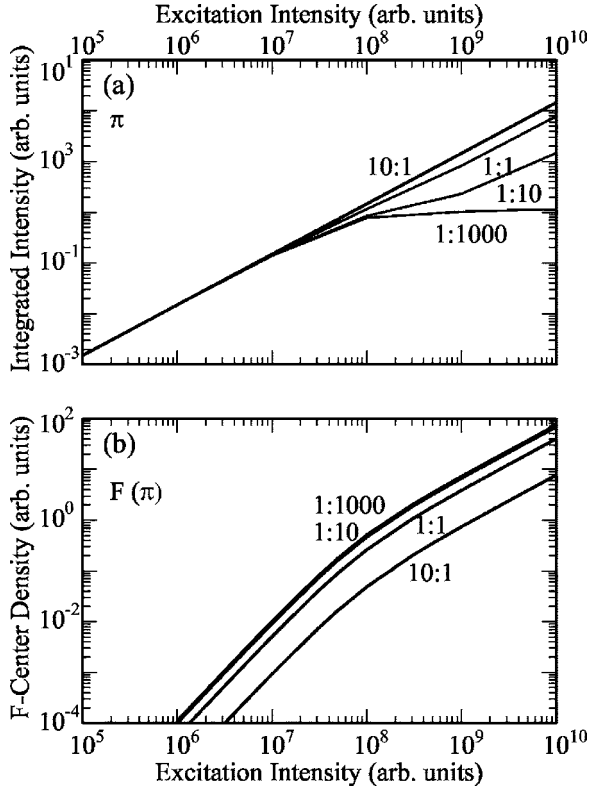
FIG. 23. (a) Integrated intensity of the STE luminescence and (b) the F-center density plotted as a function of the excitation intensity in case of the π luminescence. The ratios of $k_{30}:k_{31}$ are denoted in the figures.

ing the laser irradiation. This is because the decay time ($k_2^{-1}=1$ μs) of the π luminescence is very long as compared with the pulse duration of the ArF excitation laser. After the laser irradiation, n_4 decreases with the decay time of $k_4^{-1}=100$ ns, while n_2 decreases very slowly except for the case of Fig. 22(d). In the case of Fig. 22(d), the slow increase of n_2 in the early stage after the laser irradiation would occur because of the dominant transtion from 4 to 2. The population n_5 becomes constant after the laser irradiation. The result indicates that no F-center formation takes place in the absence of the laser irradiation.

Under weak excitation shown in Figs. 22(a) and 22(c), n_2 is much larger than n_4 and n_5. The result indicates that one-photon excitation dominates over the excitation process. In the case of the high-density excitation and the small F-center formation rate, which is presented in Fig. 22(d), n_4 overtakes n_2 around the end time of the laser irradiation. As shown in Fig. 22(b), on the other hand, in the case of the large F-center formation rate, n_4 is smaller than n_2 even under the high-density excitation. The result implies that almost all the populations at state 3 relax to state 5 and n_4 is suppressed.

Next, we simulate the dependence of the integrated intensity of the STE luminescence and the F-center density on the excitation intensity I. The integrated intensity of the STE luminescence is given by the following sum:

$$\int_0^{t_w} (k_2N_2 + k_4N_4)dt + \int_{t_w}^{\infty} (k_2n_2 + k_4n_4)dt. \qquad (24)$$
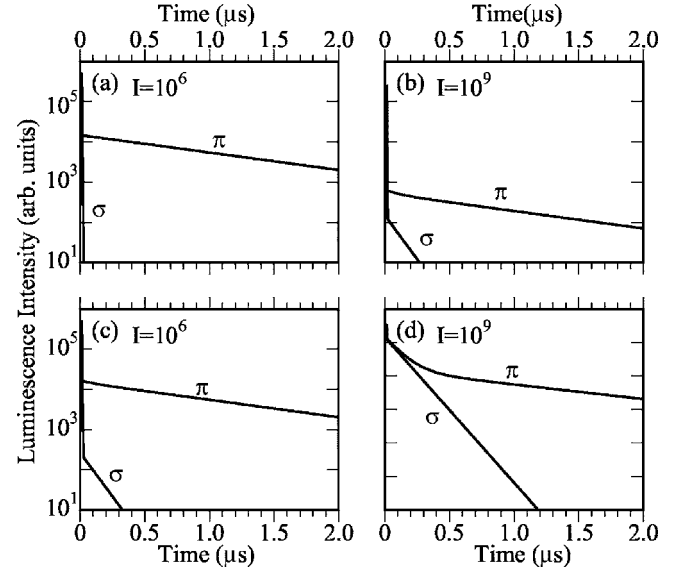
FIG. 24. Time course of the luminescence intensity of STE bands $I_s(t)$ and $I_t(t)$ after pulsed excitation. The left sides of these figures show the simulations under weak excitation, while the right sides under high-density excitation. (a) and (b) are in case of $k_{30}:k_{31}=1:1000$ and (c) and (d) are of 1:10.

On the other hand, the F-center density is simply given by $N_5(t_w)$. In case of the π luminescence, namely, $k_2^{-1}=1$ μs, the integrated intensity of the π luminescence and the F-center density are plotted as a function of the excitation intensity in Figs. 23(a) and 23(b), respectively.

Under weak excitation, the integrated luminescence intensity is proportional to the excitation intensity, and the F-center density is proportional to the second-power of the excitation intensity. Under high-density excitation and in case of the high F-center formation rate, the reduction of the luminescence efficiency is clearly observed. This result reveals that the reduction of the luminescence efficiency arises from the F-center formation. On the other hand, when the F-center formation rate is smaller, the linear relation against the excitation intensity is maintained at high intensity. The F-center formation under the high-density excitation almost quadratically depends on the excitation intensity. This result well describes the experimental result that the F-center density is proportional to $P^{1.6}$. The simulated result also demonstrates the reduction of the formation efficiency of the F centers at strong excitation.

Finally, the decay curves of the luminescence intensity of the STE $I_s(t)$ and $I_t(t)$ are simulated for $t \geqslant t_w$. The results are shown in Figs. 24(a)–24(d) for the σ and π luminescence bands. Under weak excitation, the decay components consist of the decay curves for the σ and π luminescence without the additional decay component of k_4^{-1} (100 ns). When the generation ratio of the F-center formation is large, a small amount of the decay from the paired STEs is observed and is negligibly small compared with that of a single STE. The luminescence under weak excitation is well describable in terms of a single-exponential decay, which agrees well with the experimental result under weak excitation.

Under high-density excitation and with the large F-center formation ratio $k_{30}:k_{31}=1:1000$ in the case of Fig. 24(a) in-

stead of Fig. 24(b), a single-exponential decay is observed both in the σ and π luminescence. Thus, the additional decay component is little observed. As seen in Fig. 24(d), when the *F*-center formation ratio is small, the additional decay component becomes prominent both in the σ and π luminescence. This result suggests that the rapid increase of two-photon process and the effective supply to state 4 lead to the additional decay component of the luminescence. This fact is in accordance with the simulated results in Fig. 22(d).

In general, the two-photon process involves various pathways under the high-density excitation. For example, as described before, the coherent two-photon excitation to the paired precursor state, the direct excitation of the valence electron with two-photon energy (12.8 eV), and the excitation of the electron or the hole of the STE generated by the first excitation are considered as possibilities for two-photon process. The rate equation model employed here is a typical example of many possibilities in two-photon process. Therefore, it is considered that the rate equations of Eqs. (7)–(11) describe the high-density effect only under a limited condition. Nevertheless, the model well explains three experimental results as follows. The first is the appearance of the additional decay components observed in the STE luminescence bands. The second is the reduction of the luminescence efficiency observed above ~ 0.1 mJ/cm^2. The third is the *F*-center formation which quadratically depends on the laser power.

The experimental result which cannot be explained by the present rate equation model is more than two additional decay components observed above ~ 0.1 mJ/cm^2. Since the additional decay components do not depend on laser power, some quasistable states related with the exciton relaxation newly appear under the high-density excitation. Then, more than two quasistable states might be involved in the actual relaxation process. In the present rate equation model, we take into consideration only one quasistable state corresponding to state 3.

VI. CONCLUSION

In the present study, the *F*-center formation in KI crystal under the high-density optical excitation has been investigated at low temperature. In KI crystals belonging to alkali iodides with $S/D \leqslant 0.45$, the *F*-center formation at low temperatures does not occur under the weak excitation. We have succeeded to create the *F* center in KI at 14 K. The most important experimental results obtained in this study will be summarized here. First, the *F*-center formation quadratically depends on the laser power. Second, the appearance of the additional decay components is observed in the STE luminescence bands. Third, the reduction of the luminescence efficiency is observed above ~ 0.1 mJ/cm^2. Thus, we conclude that the unusual *F*-center formation in KI at low temperature occurs via two-photon process. In addition, a simple analysis using rate equations reveals the appearance of the additional decay components in the STE luminescence bands related closely to the *F*-center formation. In our model, the paired precursor state and the paired STE state are supposed to be generated under the high-density excitation. In order to confirm our model, it is necessary to investigate the unknown states such as paired precursors and paired STEs and to clarify the dynamics under high-density excitation through the detailed experiments on the time-resolved spectroscopy of the picosecond and femtosecond time regimes.

*Present address: Nano Device Laboratory, KRI, Inc., Kyoto Research Park, Chudouji Minami-machi 134, Shimogyo-ku, Kyoto 630-8813, Japan.

[1] K. Tanimura and N. Itoh, Nucl. Instrum. Methods Phys. Res. B **32**, 211 (1988).

[2] V. H. Ritz, Phys. Rev. **133**, A1452 (1964).

[3] J. P. Duraud, F. Jollet, Y. Langevin, and E. Dooryhee, Nucl. Instrum. Methods Phys. Res. B **32**, 248 (1988).

[4] M. Szymonski, J. Kolodziej, P. Czuba, P. Piatkowski, A. Poradzisz, N. H. Tolk, and J. Fine, Phys. Rev. Lett. **67**, 1906 (1991).

[5] N. Matsunami, T. Ohwaki, N. Itoh, and Y. Horino, Nucl. Instrum. Methods Phys. Res. **194**, 39 (1982).

[6] Y. Shinozuka, Jpn. J. Appl. Phys., Part 1 **32**, 4560 (1993).

[7] K. S. Song and R. T. Williams, *Self-Trapped Exciton*, Springer Series in Solid-State Sciences Vol. 105 (Springer-Verlag, Berlin, 1993), Chaps. 5 and 6.

[8] T. G. Castner and W. Kanzig, J. Phys. Chem. Solids **3**, 178 (1957).

[9] M. N. Kabler, Phys. Rev. **136**, A1296 (1964).

[10] C. J. Delbecq, P. Pringsheim, and P. H. Yuster, J. Chem. Phys. **19**, 574 (1951).

[11] M. N. Kabler and D. A. Patterson, Phys. Rev. Lett. **19**, 652 (1967).

[12] A. M. Stoneham, J. Phys. C **7**, 2476 (1974).

[13] K. Kan'no, K. Tanaka, and T. Hayashi, Rev. Solid State Sci. **4**, 383 (1990).

[14] K. Kan'no, T. Matsumoto, and Y. Kayanuma, Pure Appl. Chem. **69**, 1227 (1997).

[15] D. Pooly and W. A. Raunciman, J. Phys. C **3**, 1815 (1970).

[16] T. Tokizaki, T. Makimura, H. Akiyama, A. Nakamura, K. Tanimura, and N. Itoh, Phys. Rev. Lett. **67**, 2701 (1991).

[17] M. Hirai, Y. Suzuki, H. Hattori, T. Ehara, and E. Kitamura, J. Phys. Soc. Jpn. **56**, 2948 (1987).

[18] S. Iwai, T. Tokizaki, A. Nakamura, K. Tanimura, N. Itoh, and A. Shluger, Phys. Rev. Lett. **76**, 1691 (1996).

[19] K. Tanimura and W. P. Hess, Phys. Rev. B **69**, 155102 (2004).

[20] Y. Kondo, M. Hirai, and M. Ueta, J. Phys. Soc. Jpn. **33**, 151 (1972).

[21] R. T. Williams and M. N. Kabler, Phys. Rev. B **9**, 1897 (1974).

[22] T. Sugiyama, H. Fujiwara, T. Suzuki, and K. Tanimura, Phys. Rev. B **54**, 15109 (1996).

[23] T. Shibata, S. Iwai, T. Tokizaki, K. Tanimura, A. Nakamura, and N. Itoh, Phys. Rev. B **49**, 13255 (1994).

[24] A. L. Shluger and K. Tanimura, Phys. Rev. B **61**, 5392 (2000).

[25] T. Karasawa and M. Hirai, J. Phys. Soc. Jpn. **39**, 999 (1975).

[26] C. B. Lushchik, G. G. Liidja, and I. Jaek, *Proceedings of International Conference Semiconductor Physics* (Czechaslovakian Academy of Sciences, Prague, 1961), p. 717.

[27] C. B. Lushchik, I. K. Vitol, and M. A. Elango, Sov. Phys. Usp. **20**, 489 (1977).

[28] B. Mizuno, K. Tanimura, and N. Itoh, J. Phys. Soc. Jpn. **55**, 3258 (1986).

[29] K. Tanimura, B. Suzuki, and N. Itoh, J. Lumin. **38**, 168 (1987).

[30] K. Tanimura, T. Eshita, and N. Itoh, J. Phys. Soc. Jpn. **53**, 2145 (1984).

[31] Y. Ban, K. Tanimura, and N. Itoh, Phys. Lett. **80A**, 53 (1980).

[32] R. T. Williams, B. B. Craig, and W. L. Faust, Phys. Rev. Lett. **52**, 1709 (1984).

[33] K. Tanimura and N. Itoh, Phys. Rev. Lett. **60**, 2753 (1988).

[34] K. Tanimura and N. Itoh, Phys. Rev. Lett. **64**, 1429 (1990).

[35] I. L. Kuusmann, P. K. Liblik, B. B. Liifya, N. E. Lushchik, C. B. Lushchik, and T. A. Soovik, Sov. Phys. Solid State **17**, 2312 (1975).

[36] C. B. Lushchik, I. Kuusmann, P. Liblik, G. Liidja, and N. E. Lushchik, J. Lumin. **11**, 285 (1976).

[37] H. Nishimura, C. Ohhigashi, Y. Tanaka, and M. Tomura, J. Phys. Soc. Jpn. **43**, 157 (1977).

[38] T. Hayashi, T. Ohata, and S. Koshino, J. Phys. Soc. Jpn. **43**, 157 (1977).

[39] C. B. Lushchik, *Excitons*, Modern Problems in Condensed Matter Sciences Vol. 2 (North-Holland, Amsterdam, 1982), Chap. 12.

[40] S. Hashimoto and M. Itoh, Jpn. J. Appl. Phys., Part 1 **27**, 726 (1988).

[41] T. Tomiki, T. Miyata, and H. Tsukamoto, Z. Naturforsch. A **29A**, 145 (1974).

[42] V. A. Kublitzky, Ann. Phys. **20**, 793 (1934).

[43] W. B. Fowler, *Physics of Color Centers* (Academic, New York, 1968), Chap. 2.

[44] T. Karasawa and M. Hirai, J. Phys. Soc. Jpn. **40**, 755 (1976).

[45] T. Okada, Radiat. Eff. Defects Solids **119-121**, 337 (1991).

[46] E. Rzepka, J. Wery, S. Lefrant, B. Ranstein, R. Tamisier, E. Hourdequin, and S. Bouffard, Nucl. Instrum. Methods Phys. Res. B **63**, 270 (1992).

[47] N. Ichimura and S. Hashimoto, J. Phys. Soc. Jpn. **68**, 1782 (1999).

[48] N. Ichimura, H. Kondo, Y. Harada, and S. Hashimoto, J. Lumin. **87-89**, 586 (2000).

[49] C. L. Bauer and R. B. Gordon, Phys. Rev. **126**, 73 (1962).

[50] T. Tsujibayashi, K. Toyoda, and T. Hayashi, Phys. Rev. B **53**, R16129 (1996).

[51] T. Tsujibayashi, K. Toyoda, and T. Hayashi, J. Lumin. **72-74**, 893 (1997).

[52] K. Toyoda, T. Tsujibayashi, and T. Hayashi, Radiat. Eff. Defects Solids **150**, 85 (1999).

[53] T. Matsumoto, T. Kawata, A. Miyamoto, and K. Kan'no, J. Phys. Soc. Jpn. **61**, 4229 (1992).

[54] M. Ikezawa and T. Kojima, J. Phys. Soc. Jpn. **27**, 1551 (1969).

[55] In our preliminary experiments for RbI, an extra luminescence band cannot be observed under the high-density excitation of the ArF excimer laser.

[56] J. U. Fishbach, D. Fröhlich, and M. N. Kabler, J. Lumin. **6**, 29 (1973).

[57] H. Nishimura, Semicond. Insul. **5**, 263 (1983).

[58] N. Ohno, S. Hashimoto, and M. Itoh, J. Phys. Soc. Jpn. **59**, 361 (1990).

[59] M. Itoh, Phys. Rev. B **35**, 7652 (1987).

[60] A. Nouaihat, G. Guillot, T. V. Khiem, and J. M. Ortega, J. Phys. (Paris), Lett. **40**, L313 (1979).